Astron. Astrophys. 315, L201–L204 (1996)

ASTRONOMY
AND
ASTROPHYSICS

The ISO/LWS far infrared spectrum of IRC+10216⋆

J. Cernicharo[1], M.J. Barlow[2], E. González-Alfonso[3], P. Cox[4], P.E. Clegg[5], Nguyen-Q-Rieu[6], A. Omont[7], M. Guélin[8], X.-W.Liu[2], R.J. Sylvester[2], T. Lim[9], M.J. Griffin[5], B.M. Swinyard[10], S.J. Unger[10], P.A.R. Ade[5], J.-P. Baluteau[11], E. Caux[12], M. Cohen[13], R.J. Emery[10], J. Fischer[15], I. Furniss[2], W.M. Glencross[2], M.A. Greenhouse[14], C. Gry[7,11], M. Joubert[16], D. Lorenzetti[17], B. Nisini[18], R. Orfei[18], D. Péquignot[19], P. Saraceno[18], G. Serra[12], C.J. Skinner[20], H.A. Smith[14], W.A. Towlson[2], H.J. Walker[10], C. Armand[9], M. Burgdorf[9], D. Ewart[9], A. Di Giorgio[9], S. Molinari[9], M. Price[9], S. Sidher[9], D. Texier[9], and N. Trams[9]

[1] CSIC. IEM. Dpto. Física Molecular, Serrano 123, E-28006 Madrid, Spain and OAN. Ap 1143, E-28800 A. de Henares, Spain
[2] Department of Physics and Astronomy, University College London, Gower Street, London WC1E 6BT, UK
[3] Universidad de Alcala de Henares, Dpto Física, Campus Universitario, E-28871 Alcalá de Henares, Madrid, Spain
[4] Institut d'Astrophysique Spatiale, Bât. 120, Université de Paris XI, F-91405 Orsay, France
[5] Queen Mary and Westfield College, University of London, Mile End Road, London E1 4NS, UK
[6] Observatoire de Paris, 61 avenue de l'Observatoire, F-75014 Paris, France
[7] Institut d'Astrophysique de Paris, 98bis Boulevard Arago, F-75014 Paris, France
[8] IRAM, Domaine Universitaire de Grenoble, 300 rue de la Piscine, F-38406 St Martin d'Hères, France
[9] The LWS Instrument-Dedicated Team, ISO Science Operations Centre, PO Box 50727, E-28080 Madrid, Spain
[10] Rutherford Appleton Lab., Chilton, Didcot, Oxon OX11 0QX, UK
[11] Laboratoire d'Astronomie Spatiale, CNRS, BP8, F-13376 Marseille, France
[12] Centre d'Etude Spatiale des Rayonnements, CESR/CNRS-UPS, BP 4346, F-31029 Toulouse Cedex, France
[13] Radio Astronomy Laboratory, 601 Cambell Hall, University of California, Berkeley, CA 94720, USA
[14] National Air and Space Museum, Smithsonian Institution, Washington, DC 20560, USA
[15] Naval Research Laboratory, Remore Sensing Division, 4555 Overlook Ave, SW, Washington, DC 20375, USA
[16] Observatorio Astronomico di Roma, I-00040 Monte Porzio, Italy
[17] CNES, 2 place Maurice Quentin, F-75001 Paris, France
[18] CNR-Instituto di Fisica dello Spazio Interplanetario, Casella Postale 27, I-00044 Frascati, Italy
[19] Observatoire de Paris, Section d'Astrophysique, F-92190 Paris, France
[20] Space Telescope Science Institute, 3700 San Martin Drive, Baltimore, MD 21218, USA

Received 17 July 1996 / Accepted 3 August 1996

Abstract. We present an ISO Long Wavelength Spectrometer (LWS) grating spectrum of the carbon-rich circumstellar envelope -CSE- of IRC+10216 between 43 and 197 μm. The spectrum consists of strong dust emission plus a forest of emission lines from CO, HCN, $H^{13}CN$ and vibrationally excited HCN (ν_2=1^1,$2^{0,2}$ and $\nu_{1,3}$=1). All the CO lines between J=14–13 and J=39–38 have been detected while lines of HCN with J_u as high as 48 have also been observed. The molecular emission arises from the warm and dense gas located in the innermost zone of the CSE. The CO and HCN emission can be easily explained if the vibrational and rotational temperatures are around 700-1500 K.

We also report the tentative detection of the bending mode of the C_3 molecule around 62 cm^{-1} (157.2 μm).

Key words: stars: AGB and post AGB – stars: individual: IRC+10216 – stars: circumstellar matter – infrared: stars

1. Introduction

IRC+10216 (CW Leo) is by far the brightest C-rich evolved object in the infrared sky. It has an extended envelope where more than 30 molecular species have been detected and it is probably one of the best studied objects at IR and mm-wavelengths (Cernicharo, Guélin and Kahane, 1996). This object has a particularly rich carbon chemistry and many of the species detected in its molecular envelope are carbon chain radicals (C_5H, C_6H, H_2C_3, H_2C_4 ,C_8H -see Cernicharo 1988 and Cernicharo and Guélin 1996) which are formed in the external layers of the CSE (Guélin, Lucas and Cernicharo 1993). The innermost regions of the envelope are dominated by a chemistry at thermodynamical equilibrium (Tsuji, 1973). Most of the stable diatomic and a few

Send offprint requests to: J. Cernicharo

⋆ Based on observations with ISO, an ESA project with instruments funded by ESA Member States (especially the PI countries: France Germany, the Netherlands and the United Kingdom) and with the participation of ISAS and NASA.

polyatomic species form there efficiently and have been detected at radio and near-infrared wavelengths (CO, HCN, C_2H_2, SiO, CS, SiS, ...). Metal-bearing molecules such as the metal halides NaCl, AlCl, AlF, KCl and MgNC have first been detected in the CSE of IRC+10216 by Cernicharo and Guélin (1987). The CSE of IRC+10216 is thus a major laboratory for the study of circumstellar and interstellar chemical processes.

In comparison with the millimeter/submillimeter domains where up to now most of the studies have been made, the far-IR range provides, together with near-IR high resolution spectroscopy, a unique opportunity to probe the inner hottest regions of the CSE. The molecular transitions at IR wavelengths involve high quantum numbers and it becomes possible to trace the molecular material in the innermost zones of the CSE. This letter presents a grating spectrum of IRC+10216 between 43 and 197 μm obtained with the LWS on board the Infrared Space Observatory (ISO). The LWS and the calibration of the spectra obtained with it are described by Clegg et al. (1996) and by Swinyard et al. (1996), respectively.

2. Observations and results

The LWS grating spectrum of IRC+10216 was obtained during revolution 198 (June 2nd 1996), using the LWS01 AOT. During this observation 20 grating scans were taken with 0.5 sec integration ramps at each commanded grating position. The spectra were over-sampled, at 1/4 of a resolution element, the latter being 0.3 μm in second order (detectors SW1–SW5; $\lambda \leq 93\ \mu$m) and 0.6 μm in first order (LW1–LW5; $\lambda \geq 80\ \mu$m). The total on-target time was 3400 sec. The flux calibration of the spectra was relative to Uranus (see Swinyard et al 1996). The smooth and strong continuum is well fitted with dust emission at a temperature of 90$\pm$10 K and an emissivity index β = 1.7$\pm$0.1. The continuum peaks at wavelengths shorter than 50 μm and decreases at longer wavelengths by more than three orders of magnitude in F_λ. The continuum appears to be smooth with no major broad feature at far-infrared wavelengths. On top of the continuum many lines are clearly seen at the longer wavelength end where the continuum emission is weakest. To illustrate the line content of IRC+10216, the spectrum minus the best fit to the continuum is shown in Fig. 1 with some of the most important lines labelled. Table 1 lists the wavelengths and fluxes of the strongest features and their identifications with CO and HCN Twenty six CO pure rotational lines have been detected in IRC+10216, from J=14–13 up to J=39-38. The CO frequencies have been calculated from the rotational constants of Farrenq et al. (1991). The CO lines are strong throughout the wavelength range of the LWS and only show a drop in the intensity levels for the highest J rotational transitions. Besides the rotational lines of CO, a forest of HCN lines from different vibrational states are detected from J=18–17 to 48–47. The HCN lines from the ground state are always accompanied by a strong line at shorter wavelengths through the full LWS range. The spacing between these lines and their frequency ratios are similar to those of HCN. Hence, the rotational constants, the mass, and the structure of the carrier of these lines must be very similar to that of HCN. After elimina-

Table 1. CO and some HCN far-IR lines in IRC+10216

λ_{obs} μm	Flux W cm^{-2}	Molecule	λ_{vac} μm	Transition
188.610	0.4 10^{-19}	HCN ν_1=1^1	188.449	J=18-17
		HCN ν_3=1^1	188.491	J=18-17
188.162	0.3 10^{-19}	HCN	188.153	J=18-17
		HCN ν_2=1^1	188.182	J=18-17 c
187.640	1.7 10^{-19}	HCN ν_2=2^0	187.511	J=18-17
187.234	2.6 10^{-19}	HCN ν_2=1^1	187.236	J=18-17 d
		HCN ν_2=2^2	187.305	J=18-17 d
187.062	1.3 10^{-19}	HCN ν_2=2^2	186.987	J=18-17 c
186.040	6.0 10^{-19}	CO	185.999	J=14-13
179.510	0.8 10^{-19}	HCN ν_1=1	179.505	J=19-18
		HCN ν_3=1	179.544	J=19-18
178.278	3.9 10^{-19}	HCN	178.276	J=19-18
		HCN ν_2=1^1	178.304	J=19-18 c
177.690	1.2 10^{-19}	HCN ν_2=2^0	177.703	J=19-18
177.385	2.2 10^{-19}	HCN ν_2=1^1	177.408	J=19-18 d
		HCN ν_2=2^2	177.474	J=19-18 d
177.080	0.7 10^{-19}	HCN ν_2=2^2	177.408	J=19-18 c
173.678	5.2 10^{-19}	CO	173.631	J=15-14
170.564	0.8 10^{-19}	HCN ν_1=1	170.556	J=20-19
		HCN ν_3=1	170.593	J=20-19
169.460	3.4 10^{-19}	HCN	169.389	J=20-19
		HCN ν_2=1^1	169.415	J=20-19 c
169.033	1.2 10^{-19}	HCN ν_2=2^0	168.878	J=20-19
168.641	2.0 10^{-19}	HCN ν_2=1^1	168.564	J=20-19 d
		HCN ν_2=2^2	168.628	J=20-19 d
168.202	0.7 10^{-19}	HCN ν_2=2^2	168.275	J=20-19 c
162.780	5.0 10^{-19}	CO	162.812	J=16-15
153.358	7.5 10^{-19}	CO	153.267	J=17-16
144.780	7.0 10^{-19}	CO	144.784	J=18-17
137.170	5.2 10^{-19}	CO	137.196	J=19-18
130.358	10.7 10^{-19}	CO	130.369	J=20-19
		HCN	130.441	J=26-25
124.206	8.3 10^{-19}	CO	124.193	J=21-20
118.610	13.2 10^{-19}	CO	118.581	J=22-21
113.484	15.9 10^{-19}	CO	113.458	J=23-22
108.840	11.1 10^{-19}	CO	108.763	J=24-23
106.144	11.0 10^{-19}	HCN	106.134	J=32-31
104.440	11.2 10^{-19}	CO	104.445	J=25-24
100.428	8.8 10^{-19}	CO	100.461	J=26-25
96.753	11.7 10^{-19}	CO	96.773	J=27-26
93.401	11.1 10^{-19}	CO	93.349	J=28-27
90.177	11.4 10^{-19}	CO	90.163	J=29-28
87.196	8.6 10^{-19}	CO	87.190	J=30-29
		HCN	87.250	J=39-38
85.076	4.6 10^{-19}	HCN	85.096	J=40-39
84.410	6.0 10^{-19}	CO	84.411	J=31-30
83.041	2.6 10^{-19}	HCN	83.047	J=41-40
81.813	4.2 10^{-19}	CO	81.806	J=32-31
79.357	7.7 10^{-19}	CO	79.360	J=33-32
		HCN	79.236	J=43-42
77.044	8.4 10^{-19}	CO	77.059	J=34-33
74.850	5.7 10^{-19}	CO	74.890	J=35-34
72.700	6.0 10^{-19}	CO	72.843	J=36-35
71.056	9.6 10^{-19}	CO	70.907	J=37-36
		HCN	71.110	J=48-47
68.975	3.5 10^{-19}	CO	69.074	J=38-37
67.310	2.1 10^{-19}	CO	67.336	J=39-38

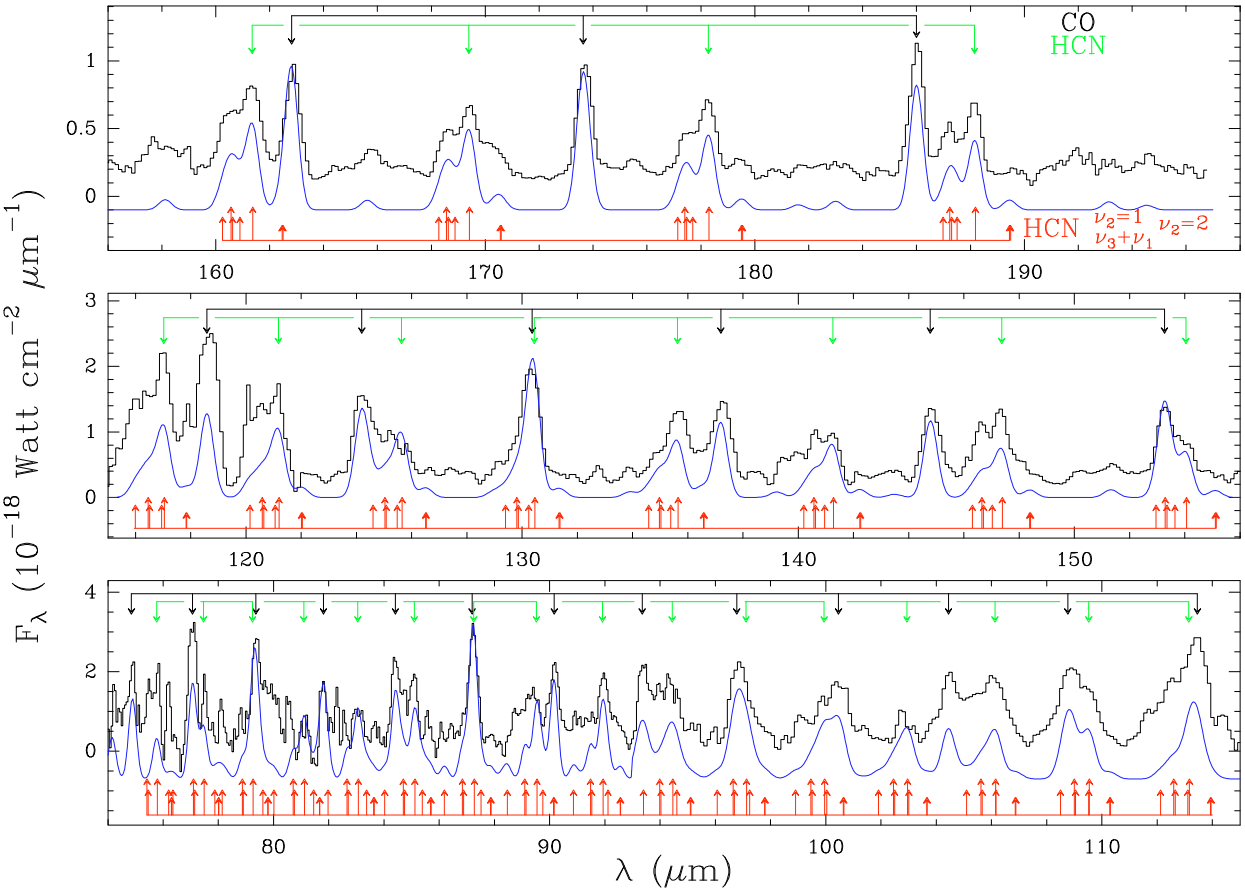

Fig. 1. Continuum subtracted LWS grating spectrum of IRC+10216 from 75 to 197 μm (thick line). An offset has been introduced to the continuum to show simultaneously the computed emission of the CO v= 0, 1, ^{13}CO v= 0, HCN and H^{13}CN v= 0, and HCN ν_2 = 1, 2 $\nu_{1,3}$= 1 (thin line). See text for the adopted model parameters. The rotational transitions of CO, HCN, and HCN ν_2=1,2 and $\nu_{1,3}$=1 are indicated by arrows at the top and bottom of each panel. The weak lines in the model correspond to H^{13}CN, ^{13}CO and to the stretching modes of HCN.

tion of a few obvious species for which the frequencies are well known (e.g. HNC), the best candidate appears to be HCN itself, but in bending vibrational excited states. HCN has a bending mode, ν_2, at ∼713 cm^{-1}, and two stretching modes ν_1 and ν_3, at 2096 and 3311 cm^{-1} respectively. From the rotational constants of De Lucia and Helminger (1977) we have computed the frequencies for HCN in different vibrational states and we conclude that after removing the CO lines, all the remaining strong features in the far-IR spectrum of IRC+10216 are due to HCN. The blue feature appearing near the HCN lines corresponds to the ν_2=1 l=1^c component, while the l=1^d is blended with HCN itself. The HCN lines have similar intensities to those of CO, a situation which is very different to what is observed in the PPN AFGL 2688 where HCN is very weak compared to CO (Cox et al. 1996). The difference between the emission in both sources can be related to their different evolutionary stages, with an important contribution to the CO emission in AFGL 2688 coming from shocked gas at moderate temperature.

Some of the weak features remaining in the far-IR spectrum of IRC+10216 could be assigned to rotational transitions of CS and SiO. However, the limited spectral resolution avoids any certain identification for these features. We have searched for NaH, MgH, CaH, NH, CH, FeH, NiH, SH, SiH, CH_2, and other light molecular species without success. However, we report a tentative detection of the Q(2,4,6,8) lines of the bending mode of triatomic carbon, C_3, around 157.2 μm (see Figure 1 top panel).

3. Discussion

The most spectacular result from the ISO/LWS spectrum of IRC+10216 is the forest of lines arising from the different vibrational levels of HCN. This result could have been expected in view of the strong maser emission found by Lucas and Cernicharo (1989) in the ν_2=1 state and the strong thermal emission in the J=2-1 and J=3-2 lines from the other vibrational levels of HCN. For a gas thermalized at 1000 K, 19% and 15% of the HCN molecules will be in the ν_2=1^1 and in the ν_2=2^{0,2} levels respectively. At 1500 K the ν_1 level will contain 5% of the HCN molecules and, together with the ν_3 level, could start to contribute to the forest of HCN lines in IRC+10216. The typical shape of the HCN lines, after convolution with the grating response, corresponds to a double peaked line (ν_2=0, 1, 2)

with a red shoulder arising from the rotational lines in excited stretching modes and a weak blue shoulder from the bending levels ν_2=3,4. From the observed intensities of the ν_2=1 l=1c components it appears that HCN rotational transitions in the ground state have intensities similar to those of the ν_2=1 levels. However, due to the large opacity of the HCN lines in the ground state, with most of them populated through the whole CSE, the observed line intensity ratios cannot be used to derive abundances for the HCN vibrational levels. The HCN opacity is so large that we have been able to detect, for the first time, a HCN l-doubling line (ΔJ=0) with the 30-m radiotelescope corresponding to J=19–19 at 84919.2 MHz (Cernicharo et al. 1996).

In order to compute the line intensities of HCN and CO we have made LVG models for their ground state and we have assumed that the vibrational levels of HCN are populated only in the inner envelope, $r < 50\ R_*$, where they are thermalized to the kinetic temperature of the gas. Taking into account the high mass loss rate of IRC+10216 these assumptions, $T_{vib}(r)=T_{gas}(r)$, seem reasonable in the inner CSE. More detailed calculations will require the collisional cross sections for vibrational transitions which are, so far, unknown. The adopted gas kinetic temperature in our models is 1200 K for $r<6\ 10^{14}$ cm and $T(r)=1200\ (6\ 10^{14}/r)^{0.7}$ for larger radii. The CO abundance is adopted to be $4.5\ 10^{-4}$ and the $^{12}C/^{13}C$ abundance ratio has been fixed to 45 (Cernicharo et al. 1991). A first analysis of the HCN lines indicate that the abundance of this molecular species must be considerably larger (around 10^{-5}) in order to fit the observed line intensities of its different vibrational states of. The adopted radius, mass loss rate, distance and terminal velocity for IRC+10216 are $3.5\ 10^{13}$ cm, $1.5\ 10^{-5}\ M_\odot\ yr^{-1}$, 200 pc, and $14.5\ km\ s^{-1}$, respectively. The inner and external radii of the CSE are taken to be $5\ 10^{13}$ and 10^{17} cm, respectively. Forty levels have been included for CO v=0, 1 and ^{13}CO v=0, and 50 levels for HCN in its different vibrational states. Collisional cross sections for CO and ^{13}CO are taken from Schinke et al. (1985). Values for J>20 have been extrapolated from the low J ones. The collisional cross sections for HCN have been adopted to be the CO values corrected for the different mass of both molecules.

The best agreement between the observations and the model results (which are shown in Figure 1) is obtained for HCN/CO=0.1 which corresponds to an HCN abundance of $3\ 10^{-5}$, a value that agrees with that derived from millimeter observations (Cernicharo et al 1987). Several lines of $H^{13}CN$ are detected corresponding to the rotational transitions J=18–17, 19–18, 21–20, 22–21, 23-22 and 26–25 Some weak and broad features present in Figure 1 could also correspond to the ν_2=1,2 levels of $H^{13}CN$. The calculated intensities for the stretching modes of HCN are understimated in our models. It could be possible to get a better fit to these lines by increasing the vibrational temperature of the ν_1 and ν_3 levels. However, that of the bending modes must be be maintained around 1000 K in order to fit the intensities of their rotational lines. Taking into account the uncertainties associated with the data calibration and with the baseline used to remove the continuum, the agreement between the observations and our model results is reasonably good. The residuals of the model–fit indicate the presence of a few strong lines without any systematic spectral pattern. One of them, at 89.2 μm agrees with a line from atomic aluminiun. However, such an identification needs confirmation from higher spectral resolution observations. In the far-IR, λ>70 μm, the power emitted in the HCN lines is 0.44 $L_\odot$ while that of CO is 0.28 $L_\odot$ (even when the millimeter and sub-millimeter lines of CO and HCN are included). Hence HCN is the main coolant of this C-rich CSE where it plays a similar role to that of water in O-rich CSEs.

References

Cernicharo J., 1988, Ph.D. Université de Paris VII

Cernicharo J., Guélin M.:1987, A.&A. 183, L10

Cernicharo J., Guélin M., Kahane C.:1996, A.&A. SS, in preparation

Cernicharo J., Guélin M., Menten K., Walmsley C.M.:1987, A.&A. 181, L1

Cernicharo J., Guélin M., Kahane C.,Bogey M., Demuynck C., Destombes, J.L.:1991, A.&A. 246, 213

Cernicharo J., Guélin M.:1996, A.&A. 309, L27

Clegg et al. 1996, A.&A. this volume

Cox et al. 1996, A.&A. this volume

De Lucia F.C., Helminger P.A. 1977, J. Chem. Phys., 67 4262

Farrenq R., Guelachvili G., Sauval A.J., Grevesse N., Farmer C.B. 1991, J. Mol. Spectrosc. 149, 375 and

Guélin M., Lucas R., Cernicharo J.:1993, A.&A., 280, L19

Lucas R., Cernicharo J. 1989, A.&A. 218, L20

Swinyard B.M. 1996, A.&A. this volume

Tsuji T.:1973, A.&A., 23, 411